



# Preparation and Characterization of Chitosan and Inclusive Compound-Layered Gold Nanocarrier to Improve the Antiproliferation Effect of Tamoxifen Citrate in Colorectal Adenocarcinoma (Caco-2) and Breast Cancer (MCF-7) Cells

Yahia KAHLOUS<sup>1</sup>, Vijayaraj Kumar PALANIRAJAN<sup>1\*</sup>, Melbha STARLIN<sup>1</sup>, Jeetendra Singh NEGI<sup>1</sup>, Shiau-Chuen CHEAH<sup>2</sup>

<sup>1</sup>UCSI University, Faculty of Pharmaceutical Sciences, Department of Pharmaceutical Technology, Kuala Lumpur, Malaysia

<sup>2</sup>UCSI University, Faculty of Medicine and Health Sciences, Department of Biochemistry, Kuala Lumpur, Malaysia

## ABSTRACT

**Objectives:** Cancer diseases have been linked to a huge number of causes that led to deaths in this century along with cardiovascular and lung diseases. Most death-leading types of cancer are colon, lung, breast, and prostate cancers. Due to the remarkable properties of gold (Au) nanocarrier, they are used to deliver and improve tamoxifen (Tam) citrate activity in Caco-2 and MCF-7 cells.

**Materials and Methods:** In this study, preparation of Au nanoparticles (NPs), zeta-potential and size, high resolution transient electron microscopy (HRTEM), high-performance liquid chromatography, ultraviolet-visible spectra, fluorescence microscopy, fourier infrared spectroscopy, and real-time cellular analysis xCELLigence technology were investigated.

**Results:** The zeta-average size of the Tam- $\beta$ -cyclodextrin ( $\beta$ -CD)-hyaluronic acid (HA)-chitosan (Chi)-Au nanocomposite is 82.02 nm with a negative zeta potential of -23.6. Furthermore, HRTEM images showed that, successful formulation of polymer shell around Au core and the Au NP shape is mostly spherical, triangle and irregular. Furthermore, the fluorescence microscope image showed proper cellular uptake of the Tam- $\beta$ -CD-HA-Chi-Au nanocomposite in MCF-7 and Caco-2 cells. Additionally, Tam- $\beta$ -CD-HA-Chi-Au nanocomposite significantly improved the cytotoxic activity of Tam citrate on Caco-2 cells. IC<sub>50</sub> value of Tam reduced from 8.55  $\mu$ M to 5.32  $\mu$ M, after 48 h of incubation time ( $p$  value <0.00001).

**Conclusion:** This study showed that Tam- $\beta$ -CD-HA-Chi-Au nanocomposite is a potential nanocarrier for delivering the drug to Caco-2 and MCF-7 cancer cells, since it has improved Tam citrate activity on colorectal cancer cells. After all, the developed formula showed more effect on Caco-2 than MCF-7. The prepared nanocomposite could be used to improve the cancer therapy in clinical trials.

**Key words:** Chitosan gold nanoparticles, tamoxifen citrate and  $\beta$ -cyclodextrin, MCF-7 cell line and Caco-2 cell line, cytotoxicity and cellular uptake, Xcelligence RTCA systems

## INTRODUCTION

Cancer diseases have been linked to a huge number of causes that lead to death in this era, along with cardiovascular and lung diseases.<sup>1</sup> Generally, cancer has widely spread in the last few years, the number of cancer patients in America alone reaches,

around 1,806,590 patients.<sup>2</sup> Most death-leading types of cancer are colon, lung, breast, and prostate cancers. Among various cancer types, colorectal cancer has a high prevalence in the United States, with 147,950 new patients and 53,200 expected deaths. Approximately 104,610 patients were identified with

\*Correspondence: vijayarajkumar\_p@yahoo.com, Phone: +60103782399, ORCID-ID: orcid.org/0000-0003-1129-7084

Received: 19.05.2021, Accepted: 17.09.2021

©Turk J Pharm Sci, Published by Galenos Publishing House.

colon cancer and 43,340 were identified with rectal cancer during 2020.<sup>3</sup> The potential causes of colon cancer may be sporadic, hereditary, or caused by the development of ulcerative colitis and Crohn's disease.<sup>4</sup>

Tamoxifen citrate (Tam) is most frequently used for treating breast cancer by preventing the estrogen hormone from binding to its receptors.<sup>5</sup> Therapeutic dose of the Tam was 10 mg 40 mg/day, while 15.2 mg of Tam citrate is equivalent to 10 mg Tam. Tumors are generally associated with irregular blood vessels with the ability to increase permeation and poor lymphatic drainage that contributes to the retention inside tumors.<sup>6</sup> This enhanced permeability and retention effect could be utilized by nanoparticles (NPs) to localize inside solid tumours.<sup>7</sup> Various nanocarriers formulations have been developed to improve chemotherapy.<sup>8</sup> Doxil and myocet (doxorubicin liposomes) were the first class therapeutics to be approved for cancer therapy.<sup>9</sup> Other promising nanocarriers either approved or in clinical trials are nab-paclitaxel (albumin NPs),<sup>10</sup> SMANCS, CRLX-101 (camptothecin NPs) and NK-105 (paclitaxel micelle).<sup>11</sup> Moreover, nanocarriers could be decorated with targeting ligands for a specific receptor in the tumour cells to improve cellular uptake.<sup>12</sup> Few nanocarriers for targeted drug delivery are also in clinical trials such as MM302 (HER-2 targeting), MBP-426 (TfR-targeting), and BIND-014 (PSMA-targeting).<sup>13</sup> In addition to therapeutic benefits, nanocarriers could also be used in cancer diagnosis. Inorganic NPs and particularly gold (Au) NPs have extensively been used extensively to improve diagnosis of cancer tissue.<sup>14</sup>

An issue to be addressed with current chemotherapy is its ineffectiveness against multidrug resistant cancer cells.<sup>15</sup> Specifically, resilience against structurally and systematically unrelated drugs is the primary concern in cancer treatment.<sup>1</sup> Cancer cells acquire resistance mainly due to the overexpression of drug efflux proteins, DNA repair activation, and apoptotic signaling modification.<sup>16</sup> High interstitial fluid pressure of tumour stroma also hinders drug penetration that results in the development of drug resistance due to less drug exposure.<sup>17</sup>

Furthermore, multidrug resistant cancer cells strongly reduce the internalization of drugs across the cell membrane with the help of P-glycoprotein efflux pumps.<sup>18</sup> Recently, scientists have started to use several unique characteristics of the extracellular tumour microenvironment like acidic extracellular pH, specific enzymes, and hypoxia condition. Chitosan (Chi) is derived from chitin by the deacetylation process. The polymer is considered Chi, when the degree of acetylation is less than 50%, which is soluble in acidic solutions.<sup>19</sup> Moreover, Chi has increased usage due to its cationic nature and mucoadhesive properties due to it is improved drug absorption capability.<sup>20</sup> Chi NPs not only can deliver hydrophilic and hydrophobic molecules but also to stabilize pharmaceutical ingredients against enzymatic degradation and thus improve the bioavailability and prolong the drug action.<sup>21</sup> This study attempts to develop a NP drug delivery system using  $\beta$ -cyclodextrin ( $\beta$ -CD)-based inclusion complexes to enhance the cellular uptake of nanocarriers and increase the internalization of Tam inside the cancer cells and improve its efficacy.

## MATERIALS AND METHODS

### Materials

Au (III) chloride 99% (Sigma-Aldrich, USA), Chi low molecular weight (Sigma-Aldrich, USA),  $\beta$ -CD >97% (Sigma-Aldrich, USA), sodium citrate tribasic dihydrate (Sigma-Aldrich, USA), hyaluronic acid (HA) sodium salt (Sigma-Aldrich, USA), Tam citrate (Sigma-Aldrich, USA), sodium tripolyphosphate (TPP) 85% (Sigma-Aldrich, USA), Dulbecco's Modified Eagle's Medium (DMEM) (ATCC, USA), phosphate-buffered saline (PBS) (ATCC, USA), trypsin-EDTA solution (ATCC, USA), penicillin-streptomycin solution (ATCC, USA), fetal bovine serum (ATCC, USA), trypsin-EDTA solution (ATCC, USA), Caco-2 (ATCC HTB-37, USA), and MCF-7 (ATCC HTB22™, USA) cell lines.

### Preparation of Tam: $\beta$ -CD inclusion compound

Tam:  $\beta$ -CD inclusion compound was prepared in a 1:1 M ratio. Briefly, Tam and  $\beta$ -CD, 10 mg for each, were completely

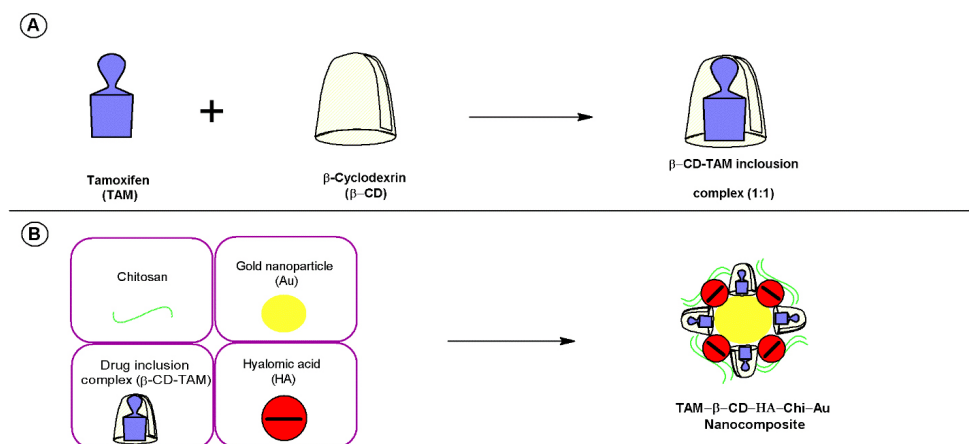


**Figure 1.** A schematic diagram describing the preparation steps of both  $\beta$ -CD-Tam inclusion complex (A) and Tam- $\beta$ -CD-HA-Chi-Au nanocomposite (B)  $\beta$ -CD:  $\beta$ -Cyclodextrin, Tam: Tamoxifen, HA: Hyaluronic acid, Chi: Chitosan, Au: Gold

dissolved in (2:1, v/v) a mixture of methanol and 30% of ammonium hydroxide. The solution was filtered through a 0.45  $\mu$  membrane filter and the filtrate was evaporated under reduced pressure and dried in a vacuum oven (80°C and 695  $\pm$  69 mbar) (Figure 1A).<sup>22,23</sup>

#### Preparation of gold nanoparticles

In brief, 2.5 mL of chloroauric acid (HAuCl<sub>4</sub>) solution (1 mg.mL<sup>-1</sup>) was mixed with 20 mL ultrapure water and the solution temperature was maintained at 80°C under magnetic stirring at 350 rpm. Then, Au NPs were formed by adding 1 mL of sodium citrate tribasic dihydrate solution (7 mg.mL<sup>-1</sup>) and stirring was continued until the colour of the solution changed to purple.

#### Preparation of chitosan-gold nanoparticles

Chi-Au NPs were prepared by adding 0.2 mL Chi solution (0.5 mg.mL<sup>-1</sup>) and 2.5 mL of HAuCl<sub>4</sub> solution (1 mg.mL<sup>-1</sup>) along with 19.8 mL of ultrapure water at 80°C and 700 rpm. Then, 1 mL of sodium citrate tribasic dihydrate solution (7.5 mg.mL<sup>-1</sup>) was added to the obtained solution and the stirring was continued until the colour of the solution changed to dark blue.

#### Preparation of Tam- $\beta$ -CD-HA-Chi-Au nanocomposite

Briefly, 12.5 mL of HAuCl<sub>4</sub> solution (1 mg.mL<sup>-1</sup>) was mixed with 1 mL Chi solution (0.5 mg.mL<sup>-1</sup>) and 97.5 mL of ultrapure water was added under stirring at 500 rpm and a temperature of 65°C for 30 min. Then, 2.5 mL of Tam- $\beta$ -CD inclusion compound and 500  $\mu$ g of HA were added to the solution. Finally, the formation of NPs was achieved by adding 3.66 mL of sodium citrate tribasic dihydrate solution (15 mg.mL<sup>-1</sup>) along with 1.84 mL of TPP solution (1 mg.mL<sup>-1</sup>) to the obtained solution under continuous stirring. The resulting NPs were centrifuged at 13,000 rpm, dried by vacuum oven (80°C and 695  $\pm$  69 mbar), and used for further studies.

#### Determination of particle size, zeta-potential and polydispersity index

Zeta-potential of Tam- $\beta$ -CD-HA-Chi-Au nanocomposite was measured by Doppler anemometry using zeta-sizer (Malvern instrument, Malvern, UK) at 25°C. Around 2 mL samples were filtered by 0.20  $\mu$ m syringe filter and then filled in the zeta cell for measuring the size and charge of the nanocomposite.

#### High resolution transient absorption microscopy (HRTEM)

HRTEM was conducted using a JEM-2100F microscope. The structure and morphology of Tam- $\beta$ -CD-HA-Chi-Au nanocomposite were determined. The sample was sonicated for 15 min. Then, one drop of the sample was placed on an HRTEM grid and maintained at room temperature of 4',6-diamidino-2-phenylindole (DAPI) until it was completely dry. After that, morphology of the nanocomposite was observed and high-quality images were taken.

#### Ultraviolet-visible (UV-visible) spectra

Optical properties of the Au NP solutions were determined using a double beam spectrophotometer by scanning the spectra from 200 to 800 nm. Sodium citrate tribasic dihydrate and TPP solution were used as the blank and ultrapure water was used

as the solvent. Au NPs, Chi-Au NPs, and Tam- $\beta$ -CD-HA-Chi-Au nanocomposite solutions were characterized as well. Fourier transform infrared spectroscopy (FTIR) spectrometers.

All spectra of the samples were taken by the Thermo Fisher Scientific Nicolet iS5 spectrophotometer (Wisconsin, USA), using OMNIC Software from 1000 to 4000 cm<sup>-1</sup> at a data acquisition rate of 2 cm<sup>-1</sup> per point.

#### Determination of encapsulation and loading efficiency

To assess the encapsulation and loading efficiency (EE) of Au NPs, 5 mg of Tam-loaded Au NPs were dissolved in methanol, then filtered and centrifuged for 30 min at 13,000 rpm.<sup>24,25</sup> The amount of Tam in the supernatant was determined by HPLC and the EE was calculated using the following equation:<sup>26</sup>

$$EE (\%) = \frac{(\text{total Tamoxifen citrate content} - \text{free Tamoxifen citrate content})}{\text{total Tamoxifen citrate content}} \times 100$$

equation 1

#### Chromatographic conditions

The HPLC system used for this study was a Waters 2487 dual  $\lambda$  absorbance detector equipped with Water 1515 Isocratic HPLC Pump and Supelco<sup>®</sup> analytical column with 15 cm x 4.6 mm *i.d.*; 5  $\mu$ m particle size. The mobile phase for gradient elution was composed of a solution of acetic acid and 1% of ammonium acetate in methanol (1:99) at 1.5 mL.min<sup>-1</sup> flow.<sup>27</sup> 10  $\mu$ L of the sample was injected into the chromatographic system.

#### Cell culture

MCF-7 (ATCC HTB22<sup>™</sup>) and Caco-2 (ATCC HTB-37) cells were routinely kept in DMEM containing 1% penicillin-streptomycin at 37°C and 10% fetal bovine serum in 5% CO<sub>2</sub> and 95% air.

#### Dynamic assessment of cytotoxic effect of Tam- $\beta$ -CD-HA-Chi-Au nanocomposites on Caco-2 and MCF-7 cells using real-time cell analysis

In this study, real-time cellular analysis (RTCA) xCELLigence technology was chosen for screening the cytopathic effect of the nanocomposite by monitoring the cellular impedance of the cells in real-time during the complete time course of the experiment.<sup>24</sup> Background measurements were taken from the wells by adding 50  $\mu$ L of DMEM media to E-plates 16. Then, MCF-7 and Caco-2 cells were seeded and plated at a density of 1x10<sup>4</sup> cells/well in fresh DMEM medium grown overnight at 37°C and 5% CO<sub>2</sub> to reach the log phase, then incubated with Tam, Tam- $\beta$ -CD-Au NPs, and Tam- $\beta$ -CD-HA-Chi-Au nanocomposite (each complex contained 23.69, 35.69, and 47.55  $\mu$ M Tam) or medium alone, and cell responses were monitored by taking RTCA DP instrument (ACEA Biosciences Inc., USA) readings every single 5 min for 24 h and every 30 min for 48 h. Kinetic profile of the cellular responses, the reduction in cell index, and IC<sub>50</sub> values as *per* each complex were taken accordingly against their respective concentrations.<sup>25</sup>

#### Preparation of rhodamine 6G-labeled Tam- $\beta$ -CD-HA-Chi-Au nanocomposite

The vacuum-dried Tam- $\beta$ -CD-HA-Chi-Au nanocomposite was redispersed in 5 mL dimethyl sulfoxide solution followed by the

addition of rhodamine 6G and 0.5 mL NaOH (0.1 M) was dissolved in methanol at 10.0 mg.mL<sup>-1</sup> concentration. The nanocomposites were incubated with rhodamine 6G solution for 24 h in the dark at environmental temperature. The prepared rhodamine-labelled Tam- $\beta$ -CD-HA-Chi-Au nanocomposites were collected by centrifugation and washed 3 times with methanol until the free rhodamine 6G could not be seen in the supernatant. Then, Tam- $\beta$ -CD-HA-Chi-Au nanocomposites were resuspended in 5 mL PBS after centrifugation.

#### Cellular uptake assessment of Tam- $\beta$ -CD-HA-Chi-Au nanocomposites by fluorescence microscopy

A Zeiss Axio Vert.A1 inverted microscope (Carl Zeiss, Germany) outfitted with HBO 50 W mercury vapor lamp and exciter/emitter filter combinations were used. Filter 38 (495 nm excitation and 517 nm emission) was used to observe FITC stained cellular membrane with green. Filter 43 (550 nm excitation and 573 nm emission) was used to observe rhodamine-labelled Tam- $\beta$ -CD-HA-Chi-Au nanocomposites with red and filter 49 (359 nm excitation and 457 nm emission) was used to observe DAPI stained cells with blue. MCF-7 and Caco-2 cells were seeded at a density of 1x10<sup>5</sup> cells/well. Then, the cells were shifted to centrifuge tubes containing serum free medium supplemented with rhodamine-labelled Tam- $\beta$ -CD-HA-Chi-Au nanocomposites (100  $\mu$ g.mL<sup>-1</sup>) and kept in the dark place for 6 h. Instantly after 6 h, the cells were washed several times with PBS and fixed by 100  $\mu$ L of 37% formaldehyde, then left at environmental temperature for 10 min followed by additional washing steps. The cells were centrifuged at 4000 rpm and the supernatant was discarded. Then, 10  $\mu$ L of DAPI stain (1  $\mu$ g.mL<sup>-1</sup>) and 10  $\mu$ L of FITC stain (60  $\mu$ g.mL<sup>-1</sup>) were added. The cells were kept in the dark place for 20 min. Finally, the cells were centrifuged and separated, then resuspended in 20  $\mu$ L of PBS and 1  $\mu$ L of cell suspension was placed onto a glass slide, then the slide was coated with a coverslip.<sup>28</sup> The images of the cells were captured, under standardized setting and contact time, a fluorescence microscope and Zen 2010 software (Blue Edition) was used for image analysis.

#### Statistical analysis

The one-way ANOVA was used to determine the significant differences between the means of three Tam- $\beta$ -CD-HA-Chi-Au nanocomposite concentrations.

## RESULTS AND DISCUSSION

#### Preparation of Tam- $\beta$ -CD-HA-Chi-Au nanocomposite

Tam- $\beta$ -CD-HA-Chi-Au nanocomposites were prepared as described by Turkevich et al.<sup>29</sup> with modification. Chi was used to offer sufficient surface area for loading the drug and improve drug delivery; hence, it was chosen to be mixed with Au (III) chloride.<sup>30</sup> Then, ultrapure water was added under stirring at 500 rpm and at a temperature of 65°C for 30 min, followed by the addition of Tam- $\beta$ -CD inclusion compound to improve Tam solubility. HA was added to enhance tumour permeability and NP retention<sup>31,32</sup> along with TPP solution, which was used as cross-linker to form electrostatic attraction between the

positively charged Chi and negatively charged TPP.<sup>33</sup> Finally, due to the reduction properties of sodium citrate tribasic dihydrate, it was added to sodium citrate tribasic dihydrate to achieve the formation of Au NPs (Figure 1B) and it resulted in the repositioning and rigidization of both inclusion compound and Chi on the superficial of Au NPs to form Tam- $\beta$ -CD-HA-Chi-Au nanocomposite.<sup>29,34</sup>

#### Particle size, zeta potential, and polydispersity index (PDI) determination

Average size of the prepared NPs was 12.31 nm with -46.4 mV zeta potential for Au NPs, 21.66 nm with -37.7 mV zeta potential for Chi-Au NPs and 82.02 nm with -32.6 mV zeta potential and PDI 0.107 (Figure 2A, B) for Tam- $\beta$ -CD-HA-Chi-Au nanocomposite (Table 1). Setyawati et al.<sup>35</sup> stated that the size of their Au NPs was 11 nm. Moreover, Regiel-Futyra et al.<sup>36</sup> reported that the size of Chi-Au NPs was 26 nm, which is similar to our average size of Chi-Au NPs. However, Kang and Ko<sup>37</sup> prepared docetaxel cationic lipid-coated Au NPs with a size of about 70 nm, which is smaller than the size of our Tam- $\beta$ -CD-HA-Chi-Au nanocomposite.

#### High resolution transmission electron microscope studies

HRTEM images revealed that the Au occupied the central position, and a layer of polymer surrounding the Au NPs that indicate a successful formulation of Au NPs and a layer of Chi and inclusion complex was deposited on the surface of NPs (Figure 3C). Figure 3A, B presents different Au NP shapes including spherical, hexagonal and irregular shapes. Regiel-Futyra et al.<sup>36</sup> reported that most of their Au NPs were in spherical shape. However, previous research reported the presence of irregular NPs with an average size of 33 nm.<sup>38</sup>

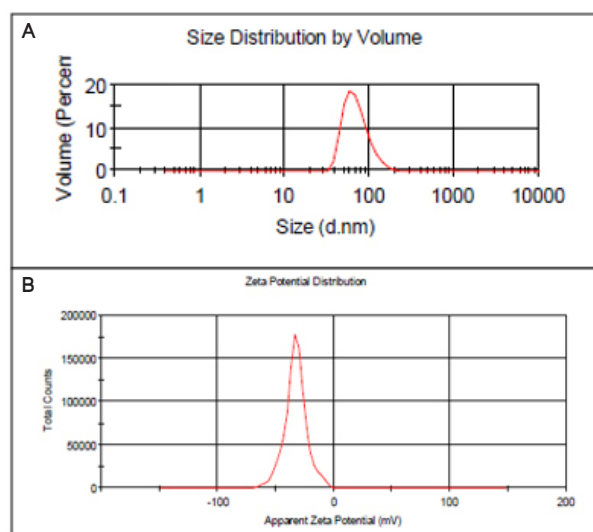


**Figure 2.** Size distribution of Tam- $\beta$ -CD-HA-Chi-Au nanocomposite by volume (A), zeta potential distribution of Tam- $\beta$ -CD-HA-Chi-Au nanocomposite (B)

$\beta$ -CD:  $\beta$ -Cyclodextrin, Tam: Tamoxifen, HA: Hyaluronic acid, Chi: Chitosan, Au: Gold

### UV-vis spectra

The reduction of  $\text{HAuCl}_4$  to Au NPs was confirmed by UV spectroscopy, by scanning the spectra from 200 to 800 nm (Figure 4D). The UV-Vis spectra of gold nanoparticles (GNPs) revealed maximum absorbance at 233 and 529 nm, which indicated that the  $\text{HAuCl}_4$  was converted to Au NPs. Whereas, when Chi was incorporated with GNPs, the result showed a shifting in  $\lambda_{\text{max}}$  from 233 to 243 and from 529 to 527 nm. Noticeably, this shifting in  $\lambda_{\text{max}}$  changed colour from purple (GNPs) to light violet (Chi-GNPs) (Figure 4A, B). However, the maximum absorbance of Tam- $\beta$ -CD-HA-Chi-Au nanocomposite was at 221 and 527 nm with a dark violet (Figure 4C) (Table 2).

### Determination of encapsulation efficiency

As previously described, the encapsulation EE of Au NPs can be calculated using equation (1), which was found to be 94.97%.

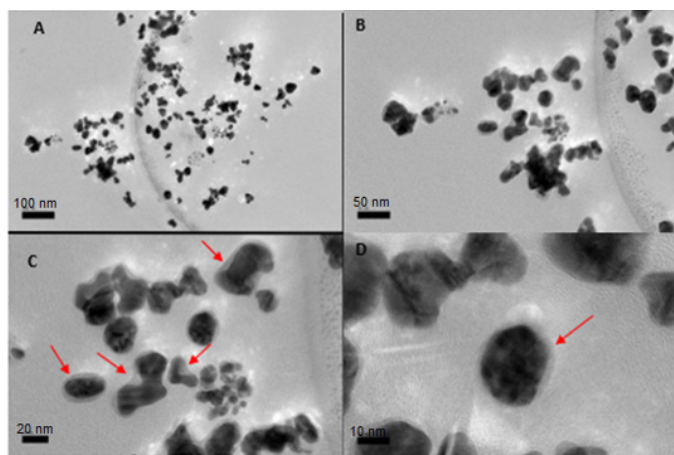


**Figure 3.** Images of Tam- $\beta$ -CD-HA-Chi-Au nanocomposite. A and B show different Au NP shapes including spherical, hexagonal and irregular. C and D show the successful formation of Chi and the inclusion complex layer that surrounded the Au NPs

$\beta$ -CD:  $\beta$ -Cyclodextrin, Tam: Tamoxifen, HA: Hyaluronic acid, Chi: Chitosan, Au: Gold, NPs: Nanoparticles

### FTIR characterization

A comparison was made of several FTIR spectra of analyzed samples to confirm the complex formation between Au NPs, Chi-Au NPs, inclusive compound, and Tam- $\beta$ -CD-HA-Chi-Au nanocomposite. Figure 5B reveals that the characteristic peak

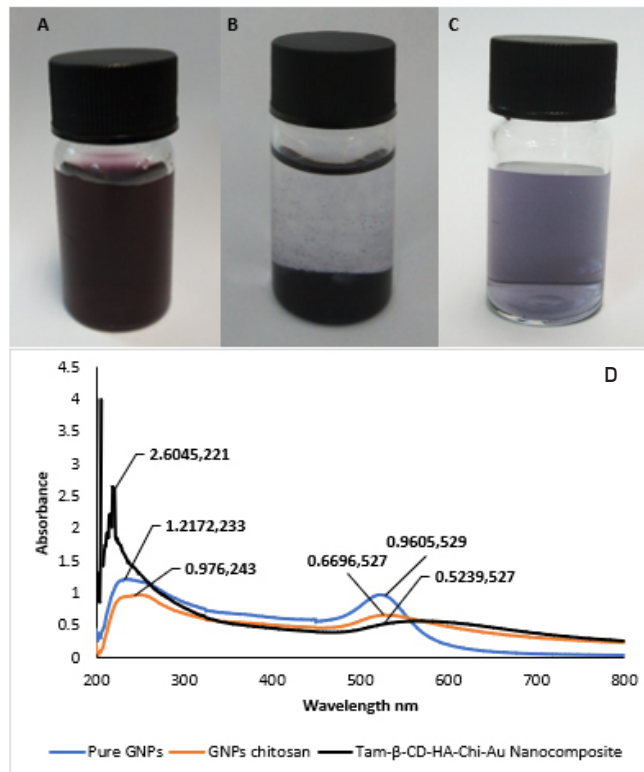


**Figure 4.** GNPs (A), Chi-GNPs (B), Tam- $\beta$ -CD-HA-Chi-Au nanocomposite (C), absorption spectra of GNPs. The results demonstrated the correlation between the shift in  $\lambda_{\text{max}}$  and the formation of NPs (D)

$\beta$ -CD:  $\beta$ -Cyclodextrin, Tam: Tamoxifen, HA: Hyaluronic acid, Chi: Chitosan, Au: Gold, NPs: Nanoparticles, GNP: Gold nanoparticles

**Table 1.** Mean particle size, zeta potential, and polydispersity index of the prepared gold nanoparticle

| Parameters         | Au NPs | Chi-Au NPs | Tam- $\beta$ -CD-HA-Chi-Au nanocomposite |
|--------------------|--------|------------|--|
| Mean particle size | 12.31  | 21.66      | 82.02                                    |
| Zeta potential     | -46.4  | -37.7      | -32.6                                    |
| PDI                | 0.544  | 0.557      | 0.107                                    |

$\beta$ -CD:  $\beta$ -Cyclodextrin, Tam: Tamoxifen, HA: Hyaluronic acid, Chi: Chitosan, Au: Gold, PDI: Polydispersity index, NPs: Nanoparticles

**Table 2.** The shift in  $\lambda_{\text{max}}$  between GNPs, Chi-GNPs, and Tam- $\beta$ -CD-HA-Chi-Au due to change in the chemical composition in nanocomposite is shown in Figure 4

| Nanoparticles                            | Absorbance (nm) |
|--|-----------------|
| GNPs                                     | 233 and 529     |
| Chi-GNPs                                 | 243 and 527     |
| Tam- $\beta$ -CD-HA-Chi-Au nanocomposite | 221 and 527     |

$\beta$ -CD:  $\beta$ -Cyclodextrin, Tam: Tamoxifen, HA: Hyaluronic acid, Chi: Chitosan, Au: Gold, GNPs: Gold nanoparticles

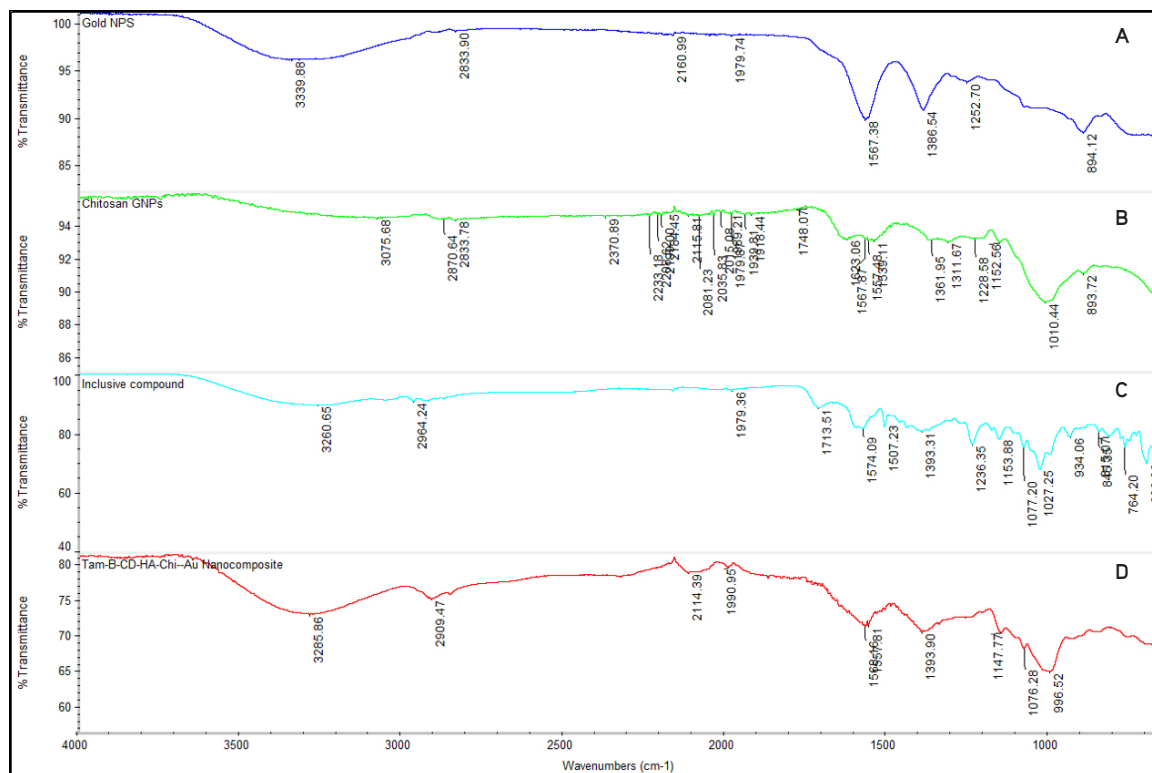


**Figure 5.** FTIR spectrum of Au NPs (A), Chi NPs (B), inclusion complex (C) and Tam- $\beta$ -CD-HA-Chi-Au nanocomposite (D)

FTIR: Fourier transform infrared spectroscopy,  $\beta$ -CD:  $\beta$ -Cyclodextrin, Tam: Tamoxifen, HA: Hyaluronic acid, Chi: Chitosan, Au: Gold, NPs: Nanoparticles

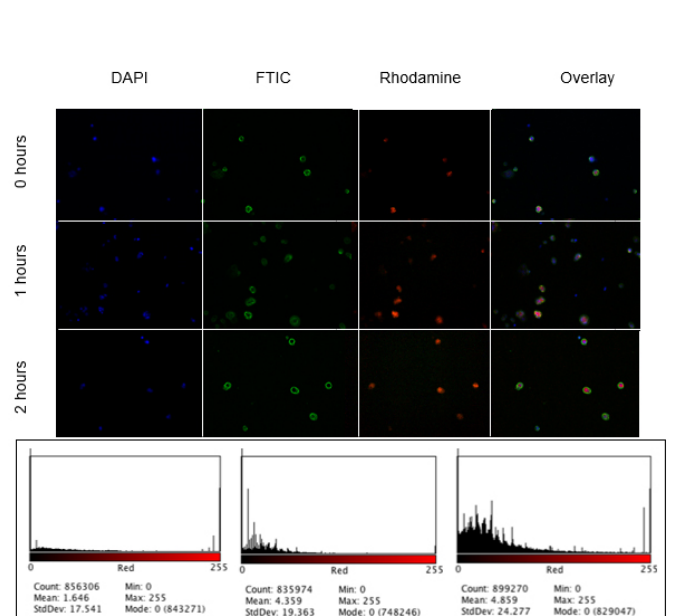


**Figure 6.** Rhodamine incorporated Tam- $\beta$ -CD-HA-Chi-Au nanocomposite uptake by Caco-2 cells. Caco-2 cells were analysed by fluorescence microscopy after 0 h, 1 h and 2 h of incubation with Tam- $\beta$ -CD-HA-Chi-Au nanocomposite (A). The red-light intensity due to rhodamine incorporated Tam- $\beta$ -CD-HA-Chi-Au nanocomposite represents the cellular uptake of the developed formulation at 0 h (B), 1 h (C) and 2 h (D)

$\beta$ -CD:  $\beta$ -Cyclodextrin, Tam: Tamoxifen, HA: Hyaluronic acid, Chi: Chitosan, Au: Gold, NPs: Nanoparticles

of Chi at  $1645\text{ cm}^{-1}$  disappeared and two new peaks appeared at  $1623\text{ cm}^{-1}$  and  $1567\text{ cm}^{-1}$ . This disappearance of the peaks can be explained by the attribution of the band to the linkage of the phosphoric and ammonium ions. This new band at  $1623\text{ cm}^{-1}$  was due to N-H vibrations in  $\text{NH}_3^+$  ion, which showed the occurrence of the cross-linking between Chi and TPP and confirmed the formation of the polyelectrolyte complex. However, the characteristic peaks of Tam in the inclusion complex entirely vanished showing characteristic peaks at  $1393\text{ cm}^{-1}$  (coupled in plane bending of  $\text{CH}_2$ ),  $2964\text{ cm}^{-1}$  (asymmetric stretching from  $\text{CH}_2$ ), and at  $3260\text{ cm}^{-1}$  (asymmetric and symmetric stretching of OH). Figure 5C indicates that the Tam molecule was entirely inserted into the  $\beta$ -CD cavity. In Figure 5D, none of the characteristic peaks of Tam nor  $\beta$ -CD were observed as the inclusive compound was loaded into the NPs, but only the characteristic peaks of Chi and Au NPs were observed with slight shifting due to the surface interaction between Chi and Au NPs.

#### Cellular uptake of Tam- $\beta$ -CD-HA-Chi-Au nanocomposite using fluorescence microscopy techniques

The objective of fluorescence microscope imaging was to confirm the cellular uptake of NPs by Caco-2 and MCF-7 cells. As shown in Figure 6A, rhodamine stained the NPs with a red and DAPI stained the nucleus with a blue, whereas fluorescein isothiocyanate stained the cellular membrane with a green. According to the data presented in Figure 6A, Caco-2 cellular uptake of Tam- $\beta$ -CD-HA-Chi-Au nanocomposite is time-

dependent. The fluorescence microscopy indicated that the Tam- $\beta$ -CD-HA-Chi-Au nanocomposite had entered the cancer cell and was localized near the nucleus. In other words, there was a portion of the Tam:  $\beta$ -CD-HA-Chi-Au nanocomposite was taken up by the cell and got localized next to the nucleus. Additionally, fluorescence images showed a punctuated staining pattern due to intracellular aggregates of the nanocomposites. Hence, cellular uptake of the prepared Tam- $\beta$ -CD-HA-Chi-Au nanocomposite was efficiently improved by Chi properties such as mucoadhesive and absorption enhancement. Moreover, the cellular uptake was also quantified by measuring the red light (due to rhodamine-labelled NPs) intensity *per* cell and as shown in Figures 6B-D (Table 3). These observations suggested that the light intensity is directly correlated with the incubation time, indicating that the developed formulation improved the cellular uptake of NPs in time-dependent manner. However, as shown in Figure 7, Tam- $\beta$ -CD-HA-Chi-Au nanocomposites did not appear at zero hour, indicating that absorption did not occur. However, at 1 h and 2 h, MCF-7 cellular uptake of Tam- $\beta$ -CD-HA-Chi-Au nanocomposite was time-dependent with a slight improvement in cellular uptake.

#### Cytotoxicity of Tam- $\beta$ -CD-HA-Chi-Au nanocomposite on Caco-2 cells and MCF-7

In this study, Caco-2 and MCF-7 cell lines were used to investigate cytotoxicity of Tam- $\beta$ -CD-HA-Chi-Au nanocomposite on cancer cells and the cellular impedance of the cells was monitored by an RTCA DP instrument. Figure 8A presents dose-dependent cytotoxicity of Tam- $\beta$ -CD-HA-Chi-Au nanocomposite on the Caco-2 cell line. Tam- $\beta$ -CD-HA-Chi-Au nanocomposite significantly improved the cytotoxic activity of Tam since the half maximal IC<sub>50</sub> value of Tam decreased from 8.55  $\mu$ M to 5.32  $\mu$ M after 48 h of incubation time (*p* value <0.00001). Since the intestinal epithelium of the small and large intestines is normally surrounded by goblet cells which secrete a thick layer of mucus around them, was postulated that the improvement in the cytotoxicity over time is due to the mucoadhesive and absorption enhancement properties of Chi. A similar study has shown that the keratinocyte growth (FGF7) FGF7:  $\beta$ -CD: Everolimus complex has a significant cytotoxicity on Caco-2 cells and has improved the antiproliferative effect of everolimus. In other words, FGF7:  $\beta$ -CD: Everolimus complex succeeded in reducing the IC<sub>50</sub> value of everolimus from 9.65  $\mu$ M to 1.87  $\mu$ M.<sup>39</sup>

**Table 3.** The intake of rhodamine-incorporated Tam- $\beta$ -CD-HA-Chi-Au nanocomposite deviation for 0 h, 1 h, and 2 h is shown in Figure 6

| Time  | 0 h (h)             | 1 h (h)             | 2 h (h)             |
|---|---------------------|---------------------|---------------------|
| Intake of rhodamine-incorporated Tam- $\beta$ -CD-HA-Chi-Au nanocomposite | 856306 $\pm$ 17.541 | 835975 $\pm$ 19.363 | 899272 $\pm$ 24.277 |

$\beta$ -CD:  $\beta$ -Cyclodextrin, Tam: Tamoxifen, HA: Hyaluronic acid, Chi: Chitosan, Au: Gold

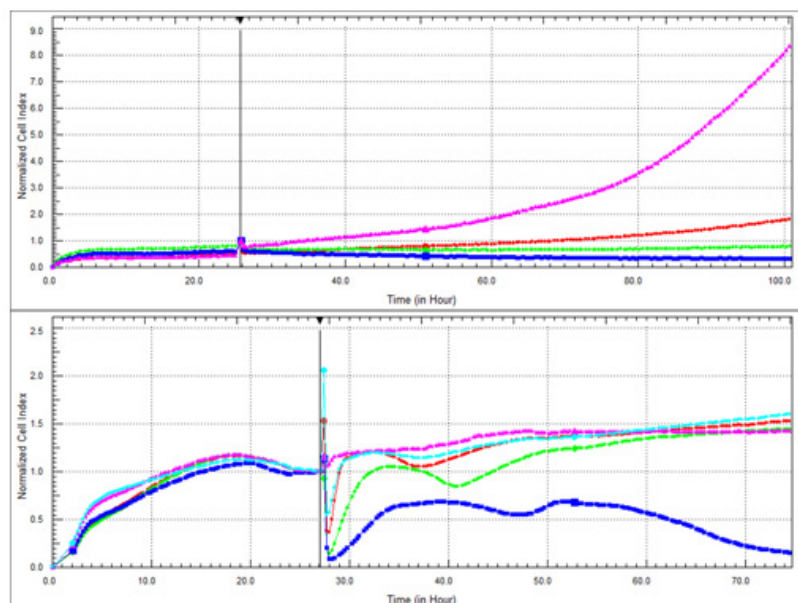


**Figure 7.** The cytotoxicity of Tam- $\beta$ -CD-HA-Chi-Au nanocomposite on Caco-2 cells is shown by the RTCA DP instrument (8A). Cells were seeded and incubated with DMEM media (1A), 23.69  $\mu$ M of Tam- $\beta$ -CD-HA-Chi-Au nanocomposite (2A), 35.62  $\mu$ M of Tam- $\beta$ -CD-HA-Chi-Au nanocomposite (3A), 47.55  $\mu$ M of Tam- $\beta$ -CD-HA-Chi-Au nanocomposite (4A). The cytotoxicity of Tam- $\beta$ -CD-HA-Chi-Au nanocomposite on MCF-7 cells is shown by the RTCA DP instrument (8B). Cells were seeded incubated with DMEM medium (pink), 2.15  $\mu$ g of Tam- $\beta$ -CD-HA-Chi-Au nanocomposite (red), 3.23  $\mu$ g of Tam- $\beta$ -CD-HA-Chi-Au nanocomposite (green), 4.31  $\mu$ g of Tam- $\beta$ -CD-HA-Chi-Au nanocomposite (dark blue), cells incubated with DMSO (light blue)

$\beta$ -CD:  $\beta$ -Cyclodextrin, Tam: Tamoxifen, HA: Hyaluronic acid, Chi: Chitosan, Au: Gold, RTCA: Real-time cellular analysis xCELLigence, DMEM: Dulbecco's Modified Eagle's Medium, DMSO: Dimethyl sulfoxide

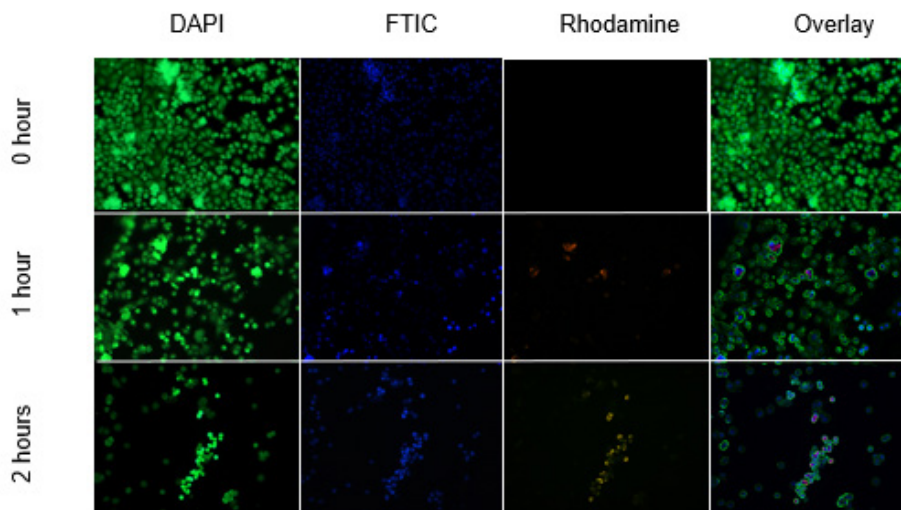


**Figure 8.** Rhodamine incorporated Tam- $\beta$ -CD-HA-Chi-Au nanocomposite uptake by MCF-7 cells was analysed by fluorescence microscopy after 0 h, 1 h, and 2 h of incubation with Tam- $\beta$ -CD-HA-Chi-Au nanocomposite. The red-light intensity due to rhodamine incorporated Tam- $\beta$ -CD-HA-Chi-Au nanocomposite represents the cellular uptake of the developed formulation at 0 h, 1 h, and 2 h

$\beta$ -CD:  $\beta$ -Cyclodextrin, Tam: Tamoxifen, HA: Hyaluronic acid, Chi: Chitosan, Au: Gold

On the other hand, no improvement in Tam cytotoxicity was observed, when the nanocomposite was tested on the MCF-7 cell line as the  $IC_{50}$  value of Tam was 6.48  $\mu$ M, which is lower than nanocomposite 68.6  $\mu$ M, after 48 h of incubation time. It is mainly due to the lack of mucus lining around MCF-7 cells, which prevents the adhesion of the nanocomposite to the cell surface and reduces the cellular uptake, and consequently affects the cytotoxicity of Tam (Figure 8B).

## CONCLUSION

Tam- $\beta$ -CD-HA-Chi-Au nanocomposite was prepared successfully, which exhibited an average size of 82.02 nm with -23.6 mV zeta potential. Au occupied the central position and a layer of polymer was surrounding Au NPs that indicates a successful formulation of Au NPs, and a layer of Chi and the inclusion complex was deposited on the surface of the NPs. Furthermore, Tam- $\beta$ -CD-HA-Chi-Au nanocomposite (equivalent to 5.32  $\mu$ M of Tam citrate) significantly improved the cytotoxic activity and cellular uptake of Tam on Caco-2 cells. However, the developed formula showed more effect on Caco-2 than MCF-7. In conclusion, this study showed that Tam- $\beta$ -CD-HA-Chi-Au nanocomposite is a potential nanocarrier to deliver the drug to cancer cells, due to its improved Tam activity on colorectal cancer cells.

## ACKNOWLEDGMENTS

This project is supported by Fundamental Research Grant Scheme (reference code: FRGS/1/2021/SKK0/UCSI/02/5), Ministry of Higher Education and Pioneer Scientists Incentive Fund Under Centre of Excellence in Research, Value Innovation and Entrepreneurship, (project code: Proj-In- FPS-017) UCSI University, Malaysia.

## Ethics

**Ethics Committee Approval:** There is no requirement for ethical approval.

**Informed Consent:** Not applicable.

**Peer-review:** Externally peer-reviewed.

## Authorship Contributions

Concept: V.K.P., Design: V.K.P., J.S.N., Data Collection or Processing: Y.K., V.K.P., M.S., J.S.N., S.S.C., Analysis or Interpretation: Y.K., V.K.P., M.S., J.S.N., S.S.C., Literature Search: Y.K., M.S., J.S.N., Writing: Y.K., V.K.P.

**Conflict of Interest:** No conflict of interest was declared by the authors.

**Financial Disclosure:** The authors declared that this study received no financial support.

## REFERENCES

- Li R, Xie Y. Nanodrug delivery systems for targeting the endogenous tumor microenvironment and simultaneously overcoming multidrug resistance properties. *J Control Release*. 2017;251:49-67.
- Bromma K, Chithrani DB. Advances in gold nanoparticle-based combined cancer therapy. *Nanomaterials (Basel)*. 2020;10:1671.
- Siegel RL, Miller KD, Goding Sauer A, Fedewa SA, Butterly LF, Anderson JC, Cercek A, Smith RA, Jemal A. Colorectal cancer statistics, 2020. *CA Cancer J Clin*. 2020;70:145-164.
- Zhao Y, Hu X, Zuo X, Wang M. Chemopreventive effects of some popular phytochemicals on human colon cancer: a review. *Food Funct*. 2018;9:4548-4568.
- Howell A, Dowsett M. Recent advances in endocrine therapy of breast cancer. *BMJ*. 1997;315:863-866.
- Maeda H, Nakamura H, Fang J. The EPR effect for macromolecular drug delivery to solid tumors: improvement of tumor uptake, lowering of

- systemic toxicity, and distinct tumor imaging *in vivo*. *Adv Drug Deliv Rev.* 2013;65:71-79.
7. Bertrand N, Wu J, Xu X, Kamaly N, Farokhzad OC. Cancer nanotechnology: the impact of passive and active targeting in the era of modern cancer biology. *Adv Drug Deliv Rev.* 2014;66:2-25.
  8. Nazir S, Hussain T, Ayub A, Rashid U, MacRobert AJ. Nanomaterials in combating cancer: therapeutic applications and developments. *Nanomedicine.* 2014;10:19-34.
  9. Barenholz Y. Doxil®-the first FDA-approved nano-drug: lessons learned. *J Control Release.* 2012;160:117-134.
  10. Reynolds C, Barrera D, Jotte R, Spira AI, Weissman C, Boehm KA, Pritchard S, Asmar L. Phase II trial of nanoparticle albumin-bound paclitaxel, carboplatin, and bevacizumab in first-line patients with advanced nonsquamous non-small cell lung cancer. *J Thorac Oncol.* 2009;4:1537-1543.
  11. A Phase III Study of NK105 in Patients With Breast Cancer: US National Library of Medicine. Available from: <https://clinicaltrials.gov/ct2/show/NCT01644890?term>
  12. Silva JM, Videira M, Gaspar R, Pr at V, Florindo HF. Immune system targeting by biodegradable nanoparticles for cancer vaccines. *J Control Release.* 2013;168:179-199.
  13. Shi J, Kantoff PW, Wooster R, Farokhzad OC. Cancer nanomedicine: progress, challenges and opportunities. *Nat Rev Cancer.* 2017;17:20-37.
  14. Thakor AS, Jokerst J, Zavaleta C, Massoud TF, Gambhir SS. Gold nanoparticles: a revival in precious metal administration to patients. *Nano Lett.* 2011;11:4029-4036.
  15. Koushik O, Rao Y, Kumar P, Karthikeyan R. Nano drug delivery systems to overcome cancer drug resistance-a review. *J Nanomed Nanotechnol.* 2016;7:378.
  16. Li W, Zhang H, Assaraf YG, Zhao K, Xu X, Xie J, Yang DH, Chen ZS. Overcoming ABC transporter-mediated multidrug resistance: molecular mechanisms and novel therapeutic drug strategies. *Drug Resist Updat.* 2016;27:14-29.
  17. Haley B, Frenkel E, eds. Nanoparticles for drug delivery in cancer treatment. *Urologic Oncology: Seminars and original investigations;* 2008: Elsevier.
  18. Creixell M, Peppas NA. Co-delivery of siRNA and therapeutic agents using nanocarriers to overcome cancer resistance. *Nano Today.* 2012;7:367-379.
  19. Akpan EI, Gbenedor OP, Adeosun SO, Cletus O. Solubility, degree of acetylation, and distribution of acetyl groups in chitosan. *Handbook of Chitin and Chitosan.* 2020:131-164.
  20. Yu S, Xu X, Feng J, Liu M, Hu K. Chitosan and chitosan coating nanoparticles for the treatment of brain disease. *Int J Pharm.* 2019;560:282-293.
  21. Shariatnia Z. Pharmaceutical applications of chitosan. *Adv Colloid Interface Sci.* 2019;263:131-194.
  22. Priotti J, Baglioni MV, Garc a A, Rico MJ, Leonardi D, Lamas MC, Menacho M rquez M. Repositioning of anti-parasitic drugs in cyclodextrin inclusion complexes for treatment of triple-negative breast cancer. *AAPS PharmSciTech.* 2018;19:3734-3741.
  23. SreeHarsha N, Hiremath JG, Chilukuri S, Aitha RK, Al-Dhubiab BE, Venugopala KN, Alzahrani AM, Meravanige G. An approach to enhance dissolution rate of tamoxifen citrate. *Biomed Res Int.* 2019;2019:2161348.
  24. Vijayakumar A, Baskaran R, Jang YS, Oh SH, Yoo BK. Quercetin-loaded solid lipid nanoparticle dispersion with improved physicochemical properties and cellular uptake. *AAPS PharmSciTech.* 2017;18:875-883.
  25. Zhang Y, Li Z, Zhang K, Yang G, Wang Z, Zhao J, Hu R, Feng N. Ethyl oleate-containing nanostructured lipid carriers improve oral bioavailability of *trans*-ferulic acid as compared with conventional solid lipid nanoparticles. *Int J Pharm.* 2016;511:57-64.
  26. Subedi RK, Kang KW, Choi HK. Preparation and characterization of solid lipid nanoparticles loaded with doxorubicin. *Eur J Pharm Sci.* 2009;37:508-513.
  27. de Santana DP, Braga RMC, Strattman R, Albuquerque MM, Bedor DCG, Leal LB, da Silva JA. Reversed phase HPLC determination of tamoxifen in dog plasma and its pharmacokinetics after a single oral dose administration. *Quim Nova.* 2008;31:47-52.
  28. Sp tL L, Sarti A, Dierich MP, M st J. Cell membrane labeling with fluorescent dyes for the demonstration of cytokine-induced fusion between monocytes and tumor cells. *Cytometry.* 1995;21:160-169.
  29. Turkevich J, Stevenson PC, Hillier J. A study of the nucleation and growth processes in the synthesis of colloidal gold. *Discuss Faraday Soc.* 1951;11:55-75.
  30. Nivethaa EAK, Dhanavel S, Narayanan V, Vasu CA, Stephen A. An *in vitro* cytotoxicity study of 5-fluorouracil encapsulated chitosan/gold nanocomposites towards MCF-7 cells. *RSC Advances.* 2015;5:1024-1032.
  31. Mattheolabakis G, Milane L, Singh A, Amiji MM. Hyaluronic acid targeting of CD44 for cancer therapy: from receptor biology to nanomedicine. *J Drug Target.* 2015;23:605-618.
  32. Prabhakar U, Maeda H, Jain RK, Sevic-Muraca EM, Zamboni W, Farokhzad OC, Barry ST, Gabizon A, Grodzinski P, Blakey DC. Challenges and key considerations of the enhanced permeability and retention effect for nanomedicine drug delivery in oncology. *Cancer Res.* 2013;73:2412-2417.
  33. Rampino A, Borgogna M, Blasi P, Bellich B, Ces ro A. Chitosan nanoparticles: preparation, size evolution and stability. *Int J Pharm.* 2013;455:219-228.
  34. Abdulkin P, Precht TL, Knappett BR, Skelton HE, Jefferson DA, Wheatley AE. Systematic control of size and morphology in the synthesis of gold nanoparticles. *Part Part Syst Charact.* 2014;31:571-579.
  35. Setyawati MI, Tay CY, Bay BH, Leong DT. Gold nanoparticles induced endothelial leakiness depends on particle size and endothelial cell origin. *ACS Nano.* 2017;11:5020-5030.
  36. Regiel-Futyra A, Kus-Li skiewicz M, Sebastian V, Irusta S, Arruebo M, Stochel G, Kyzio  A. Development of noncytotoxic chitosan-gold nanocomposites as efficient antibacterial materials. *ACS Appl Mater Interfaces.* 2015;7:1087-1099.
  37. Kang JH, Ko YT. Lipid-coated gold nanocomposites for enhanced cancer therapy. *Int J Nanomedicine.* 2015;10 Spec Iss(Spec Iss):33-45.
  38. Bindhu MR, Umadevi M. Silver and gold nanoparticles for sensor and antibacterial applications. *Spectrochim Acta A Mol Biomol Spectrosc.* 2014;128:37-45.
  39. Maki MAA, Cheah SC, Bayazeid O, Kumar PV. Cyclodextrin inclusion complex inhibits circulating galectin-3 and FGF-7 and affects the reproductive integrity and mobility of Caco-2 cells. *Sci Rep.* 2020;10:17468.